Journal of Orthopaedic Translation 52 (2025) 27–39

Contents lists available at ScienceDirect

Journal of Orthopaedic Translation

journal homepage: www.journals.elsevier.com/journal-of-orthopaedic-translation

Original Article

RO5126766 attenuates osteoarthritis by inhibiting osteoclastogenesis and protecting chondrocytes through mediating the ERK pathway

Han Wang [a,c,1], Xiwen Yuan [b,c,1], Jie Han [b,c,1], Zuoxing Wu [b,c], Zheru Ma [b,c], Fan Shi [b,c], Zhengqiong Luo [b,c], Zihan Chen [b,c], Chenyang Guo [b,c], Guixin Yuan [b,c], Xuemei He [b,c], Zemin Ling [d], Lin Meng [e], Rong Shen [a,b,*], Jianming Huang [a,**], Ren Xu [a,c,***]

[a] Department of Orthopedics, Chenggong Hospital of Xiamen University (the 73rd Group Military Hospital of People's Liberation Army), School of Medicine, Xiamen University, Xiamen, 361003, China
[b] The First Affiliated Hospital of Xiamen University-ICMRS Collaborating Center for Skeletal Stem Cell, School of Medicine, Xiamen University, Xiamen, 361000, China
[c] Fujian Provincial Key Laboratory of Organ and Tissue Regeneration, School of Medicine, Xiamen University, Xiamen, 361000, China
[d] Shenzhen Key Laboratory of Bone Tissue Repair and Translational Research, Department of Orthopaedic Surgery, The Seventh Affiliated Hospital of Sun Yat-sen University, Shenzhen, 518107, China
[e] Department of Electronic and Computer Engineering, Ritsumeikan University, Shiga, 525-8577, Japan

ARTICLE INFO

Keywords:
Chondrocyte
Degeneration
ERK pathway
Osteoarthritis
Osteoclast differentiation
RO5126766

ABSTRACT

Background: Osteoarthritis (OA) is a degenerative joint disease that remains challenging to treat due to lack of complete understanding of its pathogenesis. Previous studies have identified RO5126766 (RO) as a small molecule compound that inhibited RAF/MEK-ERK pathway and garnered much interest for its anti-cancer properties. But its role in the treatment of OA remains unclear.

Methods: This study employed the anterior cruciate ligament transection (ACLT) procedure to create an OA model in mice. The effects of RO on pathological changes in articular cartilage and subchondral bone were assessed using micro-CT and histological staining. Mice received peritoneal injections of RO at 1 mg/kg and 5 mg/kg biweekly for 4 weeks after ACLT, while control mice received saline. *In vitro*, bone marrow-derived macrophages were cultured to examine the effects of RO on osteoclast activation using immunofluorescence, TRAP staining, and bone resorption assays. The inflammatory degeneration of chondrocytes and gene expression levels were evaluated using staining and RT-qPCR. Western blot and immunohistochemistry were used to analyze MAPK signaling and autophagy-related protein expression, investigating RO's molecular mechanism in OA treatment. Human single-cell data were also analyzed to identify genes and pathways upregulated in OA tissues.

Results: Our findings showed that RO protects subchondral bone by inhibiting osteoclast formation in the ACLT mouse model of OA. *In vitro*, RO was shown to inhibit osteoclast differentiation and reduce inflammatory degeneration of chondrocytes. Mechanistically, RO counteracted subchondral osteoclast hyperactivation by suppressing the ERK/c-fos/NFATc1 signaling pathway. Additionally, RO inhibited LPS-induced inflammatory degeneration of chondrocytes and enhanced autophagy via the ERK pathway. Single-cell analysis further confirmed significant upregulation of the ERK signaling pathway in human OA tissues.

Conclusions: Overall, our findings suggested that RO inhibited osteoclast differentiation and protected articular cartilage, suggesting its potential as a novel treatment for OA.

Translational potential of this article: In this study, we have, for the first time, substantiated the therapeutic potential of RO in the treatment of OA. By demonstrating its ability to inhibit osteoclast differentiation and protect

* Corresponding author. State Key Laboratory of Cellular Stress Biology, Scholl of Medicine, Xiamen University, Yuejin Building. A503, Xiang'an South Road, Xiang'an District, Xiamen, 361102, China.
** Corresponding author. State Key Laboratory of Cellular Stress Biology, Scholl of Medicine, Xiamen University, Yuejin Building. A503, Xiang'an South Road, Xiang'an District, Xiamen, 361102, China.
*** Corresponding author. Department of, Chenggong Hospital of Xiamen University (the 73rd Group Military Hospital of PLA), No.94, Wenyuan Rd., Siming District, Xiamen, 361003, China.
E-mail addresses: Shenrong@xmu.edu.cn (R. Shen), 8303260@qq.com (J. Huang), xuren526@xmu.edu.cn (R. Xu).
[1] Han Wang, Xiwen Yuan, Jie Han have contributed equally to the work.

https://doi.org/10.1016/j.jot.2025.03.002
Received 18 July 2024; Received in revised form 9 February 2025; Accepted 13 March 2025

articular cartilage, RO could offer a new avenue for disease-modifying treatments in OA. Thus, this paper provides valuable insights into understanding the molecular mechanisms and treatment of OA.

1. Introduction

Osteoarthritis (OA) is a prevalent joint degenerative disease, characterized by the degeneration of articular cartilage, remodeling of subchondral bone, and formation of osteophyte [1–3]. It is estimated that 528 million adults worldwide were affected by OA, with approximately 133 million individuals in China experiencing OA in 2019 [4,5], placing a very heavy burden on both the individual and the community.

The pathogenesis of OA has not yet been fully elucidated, which hinders the cure for this disease. Traditional therapeutic drugs are limited to anti-inflammatory and analgesic effects but do not slow the progression of the disease [6]. In consequence, end-stage patients often require joint replacement surgery to alleviate symptoms, which is costly and risky [7]. To date, medication is still the primary form of treatment. Therefore, it is crucial to urgently clarify the mechanisms involved and explore the drugs with specific targets that can treat OA effectively.

Articular cartilage and subchondral bone play a key role in the development of OA [8]. Under normal physiological conditions, osteoblast-led bone formation and osteoclast-led bone resorption are balanced [9,10]. However, in the early stage of OA, osteoclasts-mediated bone resorption increases, and the microstructure and microenvironment of subchondral bone changes, thus altering the mechanical stress of articular cartilage and causing degeneration of articular cartilage [11,12].

In previous studies, inhibitors of various pathways such as diterbutyl phthalate, metformin, and dihydroartemisinin have been found to inhibit osteoclast generation and thus alleviate OA [13–15]. Therefore, targeting overactivated osteoclasts in subchondral bone and articular cartilage is considered as an effective and promising strategy for OA treatment. The compound RO5126766 (RO) is a potent and selective dual RAF/MEK inhibitor. In previous studies, RO has been shown to inhibit the phosphorylation of MEK by RAF and the activation of ERK by MEK [16–18].

ERK is a serine/threonine protein kinase that can be activated by cytokines produced in OA [19]. Studies have shown that ERK signaling pathway regulates various cellular processes such as cell proliferation, differentiation, apoptosis and other processes. Inhibition of ERK phosphorylation has been found to alleviate synovial inflammation and cartilage injury [20,21]. Additionally, the ERK signaling pathway up-regulates c-fos and NFATc1, which are known to play an important role in osteoclast differentiation [15,22]. Therefore, inhibiting the activation of ERK pathway can also reduce the abnormal subchondral bone remodeling induced by osteoclasts in the early stage of OA. Given the significant role of ERK pathway in OA, as well as the role of RO as an RAF/MEK inhibitor, we hypothesized that RO might function by repressing the ERK pathway.

In this study, we had this hypothesis by investigating the therapeutic effect of RO on OA degeneration in LPS-treated chondrocytes *in vitro*. Additionally, our *in vivo* study showed that intra-abdominal injections of RO at doses of 1 mg/kg and 5 mg/kg effectively reduced the severity of ACLT-induced OA. Our findings demonstrate that RO primarily inhibits osteoclast differentiation and bone resorption function, while also reducing articular cartilage destruction through the ERK pathway.

2. Materials and methods

2.1. Animals and reagents

C57BL/6J mice were acquired from Xiamen University's Study Animal Center. All mice were raised in the Experimental Animal Center of Xiamen University, with a maximum of five mice per cage under a 12-h light and dark cycle, and were fed freely. All mouse experiments were approved by the Animal Care and Use Committee of the Laboratory Animal Center of Xiamen University (XMULAC20230194).

Alpha-modified Eagle's medium (α-MEM) and penicillin/streptomycin solution were supplied by Biological Industries (BI, Beit Haemek, Israel). Fetal bovine serum (FBS) was supplied by Gibco (Thermo Fisher Scientific, Waltham, United States). Receptor Activator of Nuclear Factor-κB Ligand (RANKL) and Recombinant M-CSF were acquired from R&D Systems (Minneapolis, MN, United States). LPS was supplied by Sigma (Rainbio shanghai, China). Antibodies (p-ERK, ERK, p-p38, p38, p-JNK, JNK) were provided by Cell Signaling Technology (Danvers, United States). Anti-c-fos antibody was acquired from Abcam (Cambridge, United Kingdom). Anti-NFATc1 antibody was obtained from Santa Cruz Biotechnology (CA, United States). Anti-GAPDH antibody was acquired from Proteintech (Wuhan, China). Cell Counting Kit-8 (CCK-8) was purchased from Dojindo (Kyushu Island, Japan). RNA isolation kit was provided by Vazyme (Nanjing, China). Reverse transcription kit and real-time fluorescence quantitative polymerase chain reaction (qPCR) kit were provided by Thermo Company (Waltham, United States). Tartrate-resistant acid phosphatase (TRAP) staining kits were purchased from Sigma Aldrich (St Louis, MO, United States). Triton X-100 was purchased from Sigma Chemical (Co.St.Louis, MO, United States).

2.2. ACLT-induced OA mouse models

Studies have shown that estrogen is one of the important factors affecting the occurrence and progression of OA [23–25]. In this study, we used a male mouse model to exclude the influence of hormones and other gender-related factors from the results.8-week-old male C57BL/6J mice were randomly divided into four groups with eight mice in each group: Sham group, model group (ACLT group), low-concentration drug group (RO-1mg/kg), and high-concentration drug group (RO-5mg/kg). During the experiment, ACLT operation was performed on three groups of mice: model group, low concentration drug group and high concentration drug group. Specifically, after the mice were anesthetized with isoflurane, a longitudinal incision was made on the inside of the right knee of the mice. The joint capsule was opened under an operating microscope, the patella was peeled, and the anterior and posterior cruciate ligaments were cut. In the sham operation group, the joint capsule was opened without cutting the cruciate ligament, and the wound was sutured after the operation and penicillin powder was applied. After two weeks of modeling, the mice in the low-concentration drug group and high-concentration drug group were given peritoneal administration with the concentration of RO-1mg/kg and RO-5mg/kg, respectively. Meanwhile, the sham operation group and the model group were given the same dose of normal saline, the administration frequency was once every two days, and the total administration time was 4 weeks. After the administration, specimens were harvested.

2.3. Histology, histomorphometry, and immunohistochemistry (IHC)

Mouse knee joint tissues were harvested and were fixed with 4 % paraformaldehyde for 12 h, followed by decalcification in 10 % EDTA for 3 weeks, and then paraffin embedding and section were performed. HE staining, Safranin O-Fast Green staining and TRAP staining were performed after the section was completed following standard protocols [26]. Histomorphometric analyses were carried out using the Osteomeasure Analysis System (OsteoMetrics, Atlanta, USA) as previously described [27]. Then photographs were taken under an optical microscope, and the relative number of osteoclasts on the sections was

quantitatively analyzed by Image J software. IHC was performed as previously described [28]. Immunofluorescence staining was performed according to a previously published protocol [29].

2.4. Isolation and culture of primary bone marrow derived macrophages (BMMs)

C57BL/6J mice aged 4–8 weeks were anesthetized with 10 % chloral hydrate on the laboratory bench, then sacrificed by cervical dislocation and completely soaked in alcohol for 3 min. Under sterile conditions, the lower limb fur, muscle and other soft tissues were removed with tweezers and tissue scissors, and the femur and tibia were collected in sterile petri dishes and placed into 5 mL α-MEM medium (containing 10 % FBS+1 % penicillin/streptomycin +30 ng/mL M-CSF). The marrow cavity was rinsed with a 5 mL syringe and filtered with a 100 μm strainer into a 50 mL centrifuge tube. The centrifuge tube was centrifuged in the centrifuge for 5 min at a speed of 1500 r/min. After centrifugation, the supernatant was gently poured out, and the cells were re-suspended with 10 mL α-MEM medium (containing 10 % FBS+1 % penicillin/streptomycin+30 ng/mL M-CSF), and then transferred into T-75 culture bottle. The next experiment could be conducted after BMMs overgrew in 4–5 days.

2.5. CCK-8 assay for cell proliferation and viability

CCK-8 was used to determine the effect of RO on the proliferation and viability of ATDC5 and BMMs, according to the manufacturer's instructions. The cells were seeded in 96-well plates at densities of 5000 cells per well (ATDC5) and 6000 cells per well (BMMs) and incubated overnight. After cell adhesion, different concentrations of RO (0.5, 1, 2, 4, 8, 16 μM) were added for drug intervention, and the cells were cultured at 37 °C for 48 h. Subsequently, 10 μL CCK-8 buffer was added to each well and further incubated at 37 °C for 1.5 h. Then the OD value was scanned with a multimode scanner at 450 nm (Biotek, United States).

2.6. Histological analysis of ATDC5

ATDC5 was inoculated in clusters in a 6-well plate at a density of 20,000 cells per well. The cells were cultured in an incubator (37 °C, 5 % CO2), and after overnight adhesion, the chondrocytes were completely differentiated by DMEM medium containing 1 % ITS. LPS with a concentration of 1ug/mL was added to the positive control group and the drug group to induce the inflammatory degeneration of chondrocytes. Meanwhile, the drug group was treated with different concentrations of RO (1 μM, 2 μM) for drug intervention, and the induction medium was changed every other day. After induction to 7 and 14 days, the medium was sucked away, washed three times with PBS, fixed with 4 % paraformaldehyde for 20 min, washed twice with PBS, and then stained with Alcian blue and Safranin-O, respectively.

2.7. RNA extraction and reverse transcription-quantitative polymerase chain reaction (RT-qPCR) assay

ATDC5 was inoculated in a 6-well plate at a density of 60,000 cells per well, and the cells were cultured in an incubator (37 °C, 5 % CO2). After overnight adhesion, chondrocyte differentiation was induced by DMEM complete culture medium containing 1 % ITS, and the inflammatory degeneration of chondrocytes was induced by LPS with concentration of 1 μg/mL in the positive control group and the drug group. Meanwhile, the drug group was treated with different concentrations of RO (1 μM and 2 μM) for drug intervention, and the induction culture medium was changed every other day. After induction for 7 days, cells were collected and total RNA was extracted according to Vazyme's RNA isolation kit. Complementary DNA (cDNA) is synthesized from 1 μg total RNA and is reverse-transcribed according to Thermo's reverse transcription kit. After cDNA was prepared, qPCR assay was performed using the qPCR kit provided by Thermo Company. Quantitative expression of genes related to inflammatory degeneration in chondrocytes by qPCR. qPCR reaction conditions were 94 °C, denaturation for 2 min, 56 °C for 30s, 72 °C for 35s, 76 °C for 2s, a total of 40 cycles. The primer sequences are presented in Supplementary Table 1. All reactions were run in triplicate and GAPDH or β-Actin was used as the quantitative internal control gene. Each group was performed in triplicate, and the expression levels of the genes were quantified by the 2-ΔΔCq method [30].

In bone metabolism, RANKL is primarily produced by osteoblasts and promotes the differentiation and activation of osteoclasts, leading to bone resorption [31]. To detect the effect of RO on osteoclast-specific gene expression, BMMs was inoculated on 6-well plates at a density of 100,000 cells per well. After the cells were stuck overnight, RANKL (100 ng/mL) was added to the positive control group and the drug group on the second day to stimulate osteoclastic differentiation, while the drug group was added with different concentrations of RO (10, 20, 39 nM) for intervention, and the fluid was changed once every 2 days. The cells were cultured for about 6 days for RNA extraction and later RT-qPCR assay. The procedure is similar to ATDC5.

2.8. Osteoclastogenesis assay

BMMs was inoculated on 96-well plates at a density of 6000 cells per well, with 3 holes per concentration. After 24 h culture and cell adhesion, osteoclast differentiation was induced by α-MEM medium (containing 10 % FBS+1 % penicillin/streptomycin+30 ng/mL M-CSF) stimulated by 100 ng/mL RANKL. The positive control group and drug group were set up, in which different concentrations of RO (10, 20, 39 nM) were added to the drug group, and the culture medium was changed every 2 days. TRAP staining was performed after cell culture for about 5 days until osteoclasts were formed. The number of osteoclasts in each pore was counted (TRAP positive and $\geq$3 nuclei were considered osteoclasts).

2.9. Bone resorption assay

BMMs were inoculated on 6-well plates at a cell density of 150,000 cells per well. After incubation overnight, RANKL (100 ng/mL) was added to each well to stimulate osteoclast differentiation, and the culture medium was changed every 2 days until osteoclasts were formed. Osteoclasts were inoculated on 96-well plates containing bovine bone slices, with 3 holes for each group of drug concentration. After the cells were cultured overnight, RANKL (100 ng/mL) was added to stimulate osteoclast differentiation in each group. A positive control group was set up, and different concentrations of RO (10, 20, 39 nM) were added to the drug group. The fluid was changed every other day and cultured until bone defects formed. Then, the culture medium was sucked away, the bone slices were removed, and the cells on the bone slices were cleaned with a toothbrush, dried and photographed under electron microscope. The Image J software was used to calculate the area proportion of bone resorption lacunae.

2.10. Immunofluorescence assay for podosome belts

BMMs was inoculated in 96-well plates with a cell density of 6000 cells per well and incubated overnight in an incubator (37 °C, 5 % CO2). After the cells were attached to the wall, they were stimulated with complete α-MEM medium containing 30 ng/mL M-CSF and 100 ng/mL RANKL. At the same time, different concentrations of RO (10, 20, 39 nM) were used for drug intervention, and the culture medium was changed every 2 days. After cell culture for about 6 days until osteoclast formation, the cells were fixed with 4 % PFA, and then the cells were permeated with 0.1 % Triton X-100 for 5 min. To block non-specific immune reactivity, cells were incubated with PBS containing 3 % BSA

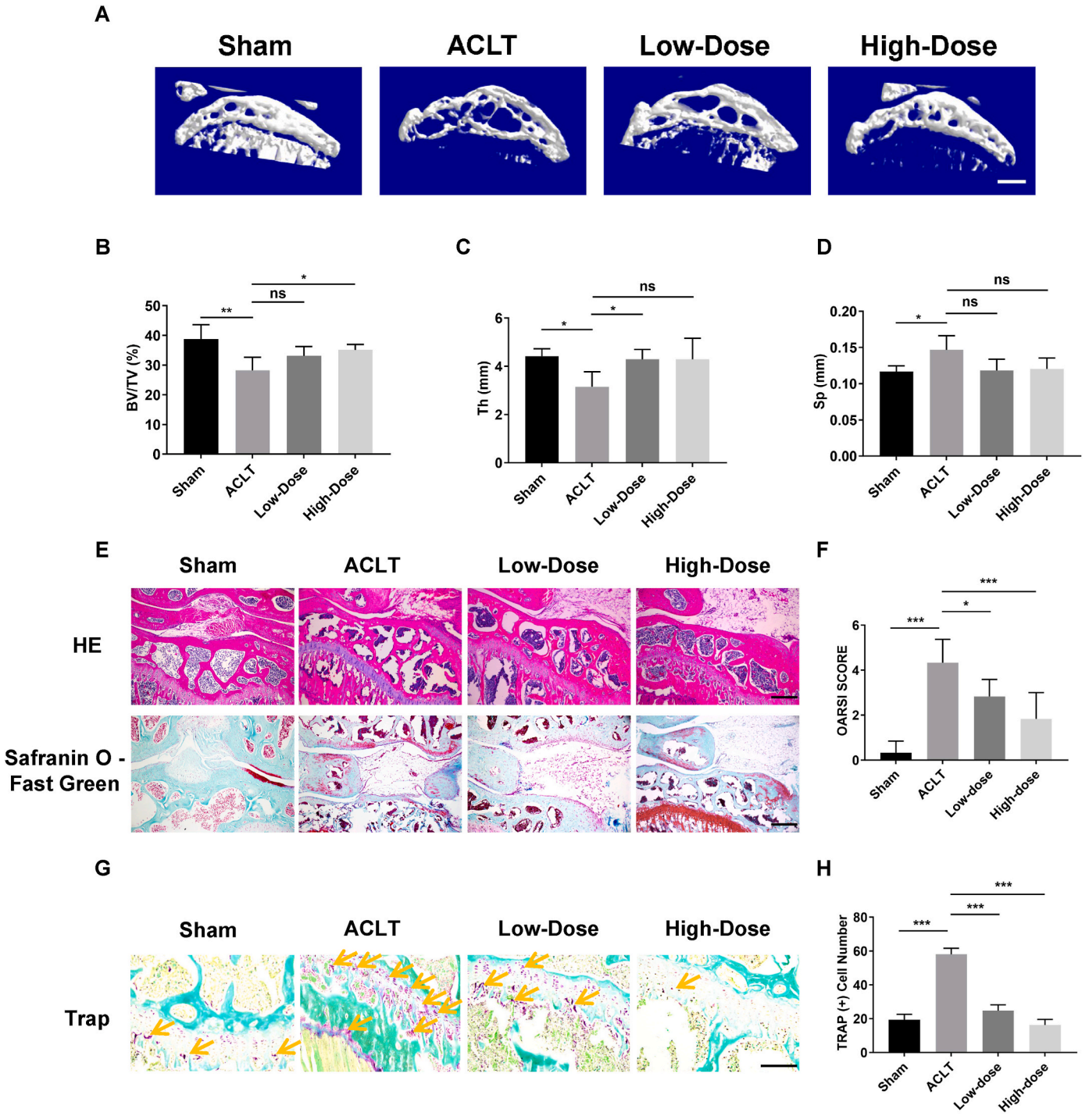

Fig. 1. RO alleviated articular cartilage degradation and subchondral osteolysis in ACLT mice. (**A**) Three-dimensional image of the sagittal plane of medial tibial subchondral bone structure at 6 weeks after operation. Scale bar = 200 μm; (**B-D**) Micro-CT quantitative analysis of tibial subchondral bone of bone volume/tissue volume (BV/TV, %) (**B**), subchondral bone plate thickness (Th) (**C**) and percent of porosity (Sp) (**D**); (**E**) HE and Safranin O-Fast Green staining at 6 weeks after ACLT. Scale bar = 200 μm. (**F**) OARSI scores of the knee joints of mice after surgery according to histological analysis; (**G-H**) TRAP staining and quantitative analysis of TRAP-positive osteoclast in subchondral bone at 6 weeks post operation. Scale bar = 100 μm. Data represent mean ± SD. N = 6 per group; *p < 0.05, **p < 0.01, ***p < 0.001. High-dose: 5 mg/kg, and Low-dose: 1 mg/kg.

for 30 min. After being washed twice with PBS containing 0.2 % BSA, the cells were incubated with rhodamine conjugated phalloidin for 1–2 h without light. The cells were washed 4 times with PBS containing 0.2 % BSA, followed by 4 times with sterile PBS. In order to display the nucleus, the cells were re-stained with DAPI under light-free conditions. Finally, after being washed with sterile PBS, the cells were imaged fluorescently using a confocal microscope.

2.11. Micro-CT analysis

The fixed mouse knee joint was placed on Skyscan 1174 Micro-CT for scanning. The parameters were set as: voltage 50Kv, current 800 μA, scanning range 2cm × 2 cm, scanning layer thickness 9 μm. After the scan, 3D reconstruction was performed using NRecon software, and CTAN software was used to analyze the tissue-related parameters of the

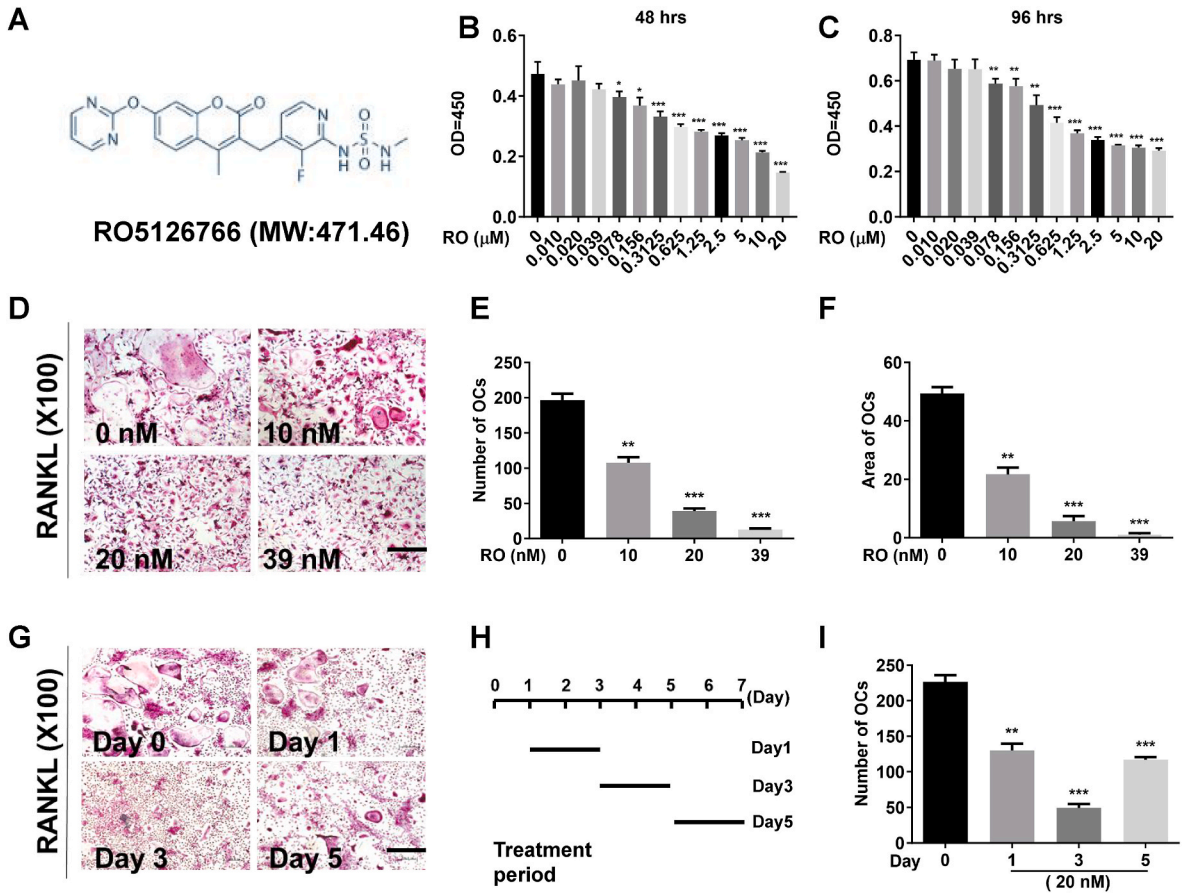

Fig. 2. RO inhibited osteoclastogenesis in vitro. (**A**) Structure formula of RO5126766; (**B, C**) Toxicity detection of RO for BMMs at 48h (**B**) and 96h (**C**). (**D-F**) TRAP staining (**D**) and quantitative analysis (**E-F**) of osteoclasts induced from BMMs. BMMs cells cultured with RANKL, treated with various levels of RO (0, 10, 20, 39 nM). Scale bar = 100 μm. (**G-I**) TRAP staining (**G**), treatment period (**H**) and quantitative analysis (**I**) of osteoclasts induced from BMMs. BMMs cells cultured with RANKL, treated with various time period (Day1, Day 3, Day5). Scale bar = 100 μm. Data represent mean ± SD. N = 3 per group; *p < 0.05, **p < 0.01, ***p < 0.001 compared with RANKL group.

reconstructed subchondral bone, including bone volume fraction (bone volume/tissue volume, BV/TV), trabecular thickness (Th), and percent of porosity (Sp). A region of interest was identified as the portion (3.5 mm ventro-dorsal length, 0.5 mm below the growth plate and 1 mm in height) of the load-bearing region at the medial tibial plateau to use for determination of the bone parameters, including bone volume fraction (BV/TV).

2.12. Western blot analysis

ATDC5 was induced to differentiate into chondrocytes by induction of DMEM medium containing 1 % of ITS, followed by inflammatory degeneration induced by LPS, and intervention with RO drugs. Cultured cells were lysed with RIPA buffer containing protease inhibitors and phosphatase inhibitors. The whole process was conducted according to standard protocols [32]. 8 % or 12 % sodium dodecyl sulfate-polyacrylamide gel electrophoresis were used to resolve the total protein, and the separated proteins were transferred to polyvinylidene difluoride membranes. Then the membranes were blocked with 5 % non-fat milk for 2 h and incubated overnight at 4 °C with primary antibodies against p-ERK, ERK. BMMs were stimulated to differentiate into osteoclasts by RANKL. After the intervention of osteoclasts with RO drugs, western blot analysis was performed, which was similar to the ATDC5 mentioned above. The primary antibodies were against p-ERK, ERK, p-p38, p38, p-JNK, JNK, NFATc1, c-fos (Supplementary Table 2). After being washed with Tris-buffered saline containing Tween-20, the membranes were incubated with secondary antibodies (mouse or rabbit). Protein bands were visualized with image quantla-4000 imaging system (GE Healthcare, Chicago, Illinois, United States), then the results were analyzed by the ImageJ software.

2.13. Statistical analysis

GraphPad Prism (v6.0a; GraphPad, La Jolla, CA, USA) was used for the statistical analyses. Experiments were repeated at least three times, and the data are expressed as the mean ± standard deviation. A two-tailed Student's t test was used to determine the significance for comparison of only two groups. $P < 0.05$ was considered to indicate a statistically significant difference.

2.14. Single cell analysis of human articular cartilage

Single-cell RNA sequencing data (GSE255460) originates from human articular cartilage tissues [33]. These data underwent comprehensive processing and quality control using Seurat (Version 5.1.0). Initially, Seurat objects were generated using the CreateSeuratObject function, with an initial cell filter removing cells with fewer than 500 genes and those exceeding a 20 % mitochondrial gene percentage. DoubletFinder was utilized to identify and eliminate doublet cells, ensuring data accuracy and reliability. Subsequently, data normalization was performed using the NormalizeData function, followed by the selection of highly variable genes with the FindVariableFeatures function. To address batch effects and integrate the data, the Harmony package (Version 0.1) was applied, resulting in an integrated dataset

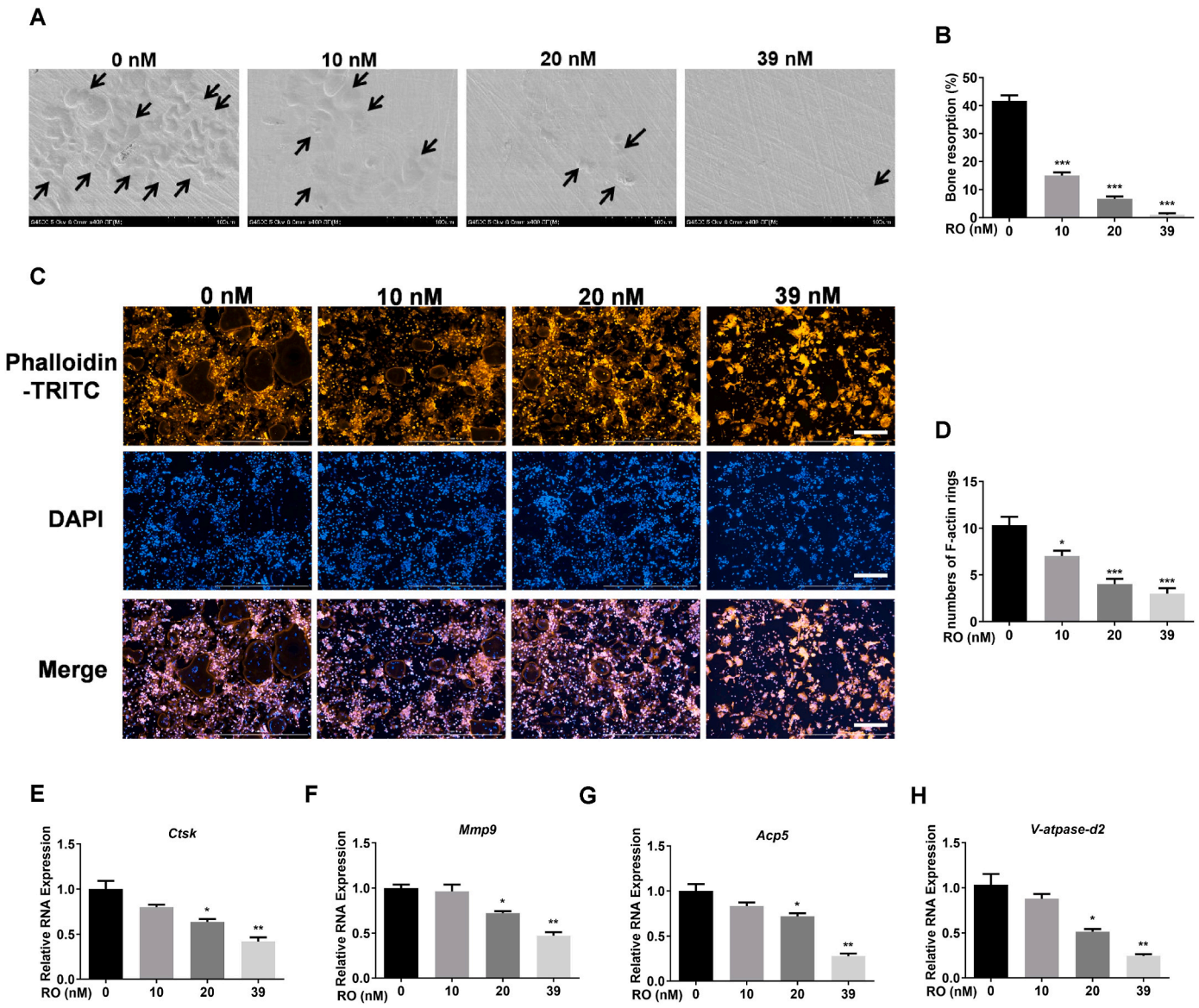

Fig. 3. RO inhibited the bone absorption function of osteoclasts. (**A**) Bone resorption pits were shown by SEM. Scale bar = 100 μm. (**B**) Quantitative analysis of resorption pits. (**C**) BMMs were stimulated with 30 ng/mL MCSF, 100 ng/mL RANKL and various concentrations of RO (0, 10, 20, 39 nM) for 6 days, before being stained with tetraethyl rhodamine isothiocyanate-conjugated phalloidin and DAPI to indicate the podosome belts and nucleus. Scale bar = 100 μm. (**D**) Quantitative analysis of F-actin rings. (**E-H**) Osteoclasts specific gene expression difference in various levels of RO (0, 10, 20, 39 nM). Data represent mean ± SD. N = 3 per group; *p < 0.05, **p < 0.01, ***p < 0.001.

comprising 133,337 cells. Further clustering analysis identified four distinct populations: articular chondrocytes (ArtiChon), osteoblasts (OsteoB), endothelial cells (Endo), and immune cells (Immune), visualized using Uniform Manifold Approximation and Projection (UMAP). Marker gene expression across each cluster was visualized using DotPlot, FeaturePlot, and vlnPlot functions in Seurat. Heatmaps, generated with pheatmap, highlighted the top 20 significantly differentially expressed genes in each cluster. For pathway enrichment analysis, the enrichPathway function from the clusterProfiler package (Version 4.0) was utilized, presenting results via barplots and dotplots. GSEA (gene set enrichment analysis) revealed significant upregulation of the ERK pathway in OA using GSEA_linux (Version 4.3.3). Furthermore, analysis with the scMetabolism package demonstrated significantly higher AUCell scores for the ERK pathway in OA samples compared to normal samples.

3. Results

3.1. Alleviation of articular cartilage degradation and subchondral osteolysis by RO in ACLT mice

RO is a potent and selective dual RAF/MEK inhibitor with a molecular weight of 471.46 (Fig. 2A) [18]. The degeneration of articular cartilage is one of the prominent features of OA [34]. To explore the effect of RO on osteoclast in subchondral bone, Micro-CT scanning was used to assess the changes of subchondral bone's microstructure of tibia. After scanning, we analyzed and compared the tissue-related parameters of the reconstructed subchondral bone. Compared with sham group, the rate of BV/TV and subchondral bone plate thickness (Th) was decreased significantly in ACLT mice. These suggest that overactivation of osteoclasts caused damage to the subchondral bone. Interestingly, the use of RO has a tendency to normalize these indicators to Sham group. It indicates that using RO makes the structure of the subchondral bone more

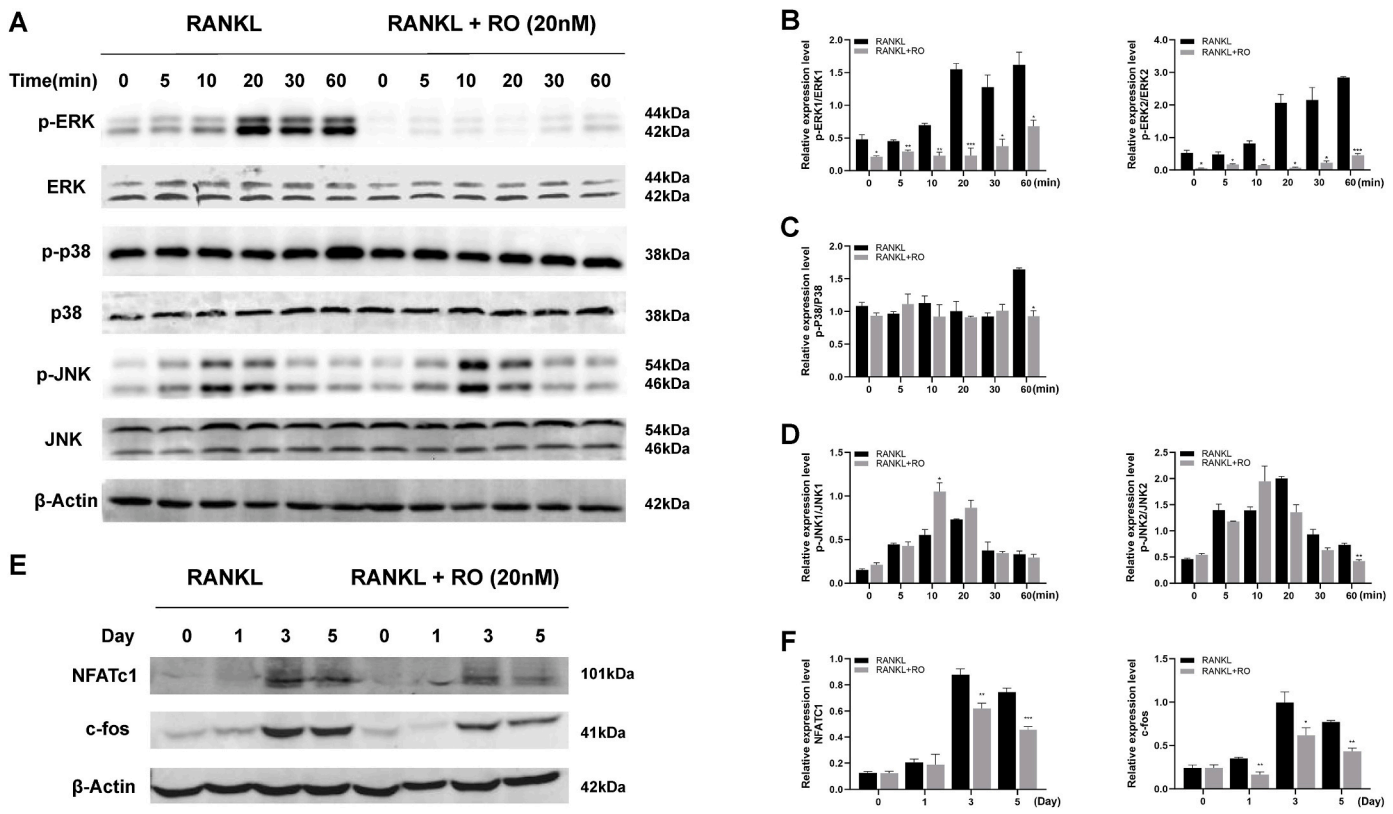

Fig. 4. RO blocked osteoclast fusion by suppressing RANKL-induced activation of ERK/c-fos/NFATc1 pathway. (**A-F**) BMMs were pretreated with or without RO (20 nM) for 3h and then stimulated with 30 ng/ml M-CSF and 100 ng/mL RANKL for indicated time period (0, 5, 10, 20, 30, 60 min, and 0, 1, 3, 5days), and the cell lysates were quantitatively analyzed using western blot for MAPK signaling pathways (**A-D**), NFATc1 and c-fos (**E-F**) signaling pathways. Data represent mean ± SD. N = 3 per group. *p < 0.05, **p < 0.01, ***p < 0.001.

stable and resistant to deformation, thus delaying the progression of OA (Fig. 1A–D).

To analyze the effect of RO on ACLT-induced OA degeneration, HE staining and Safranin O-Fast Green staining was performed 6 weeks after ACLT. Safranin O-Fast Green staining revealed significant subchondral bone collapse and erosion in the ACLT group compared to the other groups. HE staining demonstrated disrupted bone continuity in the ACLT group relative to the subchondral bone surface. In the ACLT group, inflammatory cell numbers increased significantly, normal cell counts decreased, and cell arrangement became disorganized (Fig. 1E). The above results show that the subchondral bone in the model group had obvious erosion and the cartilage had significant inflammatory degeneration. At the same time, through the treatment of RO, these traits have been significantly alleviated (Fig. 1E). The OARSI score in the ACLT group was significantly higher than in the other groups ($P < 0.01$). RO treatment effectively reduced the OARSI score and alleviated arthritis symptoms in mice after ACLT (Fig. 1F). In addition, TRAP staining confirms that osteoclasts were overactivated in the subchondral bone of mice after ACLT surgery while RO effectively reduced the number of osteoclasts (Fig. 1G and H). These results further suggest that RO has an anti-osteoclast effect. Through all these data, it demonstrates that overactivation of osteoclasts and osteolysis in subchondral bone caused by ACLT can be prevented by RO.

3.2. *RO suppresses RANKL-induced osteoclastogenesis*

To further confirm the effect of RO on osteoclastogenesis, BMMs were induced *in vitro*. First, we detected the toxicity of RO to BMMs by CCK-8 assay. It shows that RO has no significant toxicological effect on BMMs when its concentration was below 0.039 μM (Fig. 2B and C). Next, TRAP assay was conducted and it shows that RO can effectively restrain the formation of osteclasts induced by RANKL-stimulated BMMs. Through the decline of number and area of osteclasts, it proved that the differentiation of osteoclasts was significantly inhibited by RO treatment (10, 20, 39 nM) in a dose-dependent manner. As the dose increases, fewer and fewer multi-nuclear osteoclasts could be induced (Fig. 2D–F). At the same time, we examined the effect of RO treatment time on osteoclasts differentiation. In the same dose, changing the treatment period (Day1, Day3, Day5) has varying degrees inhibition, especially D3 (Fig. 2G–I).

3.3. *RO suppresses RANKL-induced bone resorption and osteoclast marker gene expression*

The bone resorption capacity of osteoclasts can be evaluated by bone slice resorption test. As the concentration of the RO increased, the area of bone resorption on the bone slice appeared to decrease significantly (Fig. 3A and B). The effect of RO on osteoclasts was further investigated by staining with TRITC-conjugated phalloidin. The group without RO had distinct podosome belts. However, treatment with different levels of RO resulted in marked alterations in the number and morphology of podosome belt. It suggested that RO inhibited podosome belts formation in osteoclasts *in vitro* (Fig. 3C,D). The expression levels of genes associated with osteoclastogenesis and function were then examined, including *Ctsk*, *Mmp9*, *Acp5*, *V-atpase-d2* [35,36]. Interestingly, the expression levels of these genes were significantly inhibited in a dose-dependent manner in the groups treated with various concentrations of RO (Fig. 3E–H).

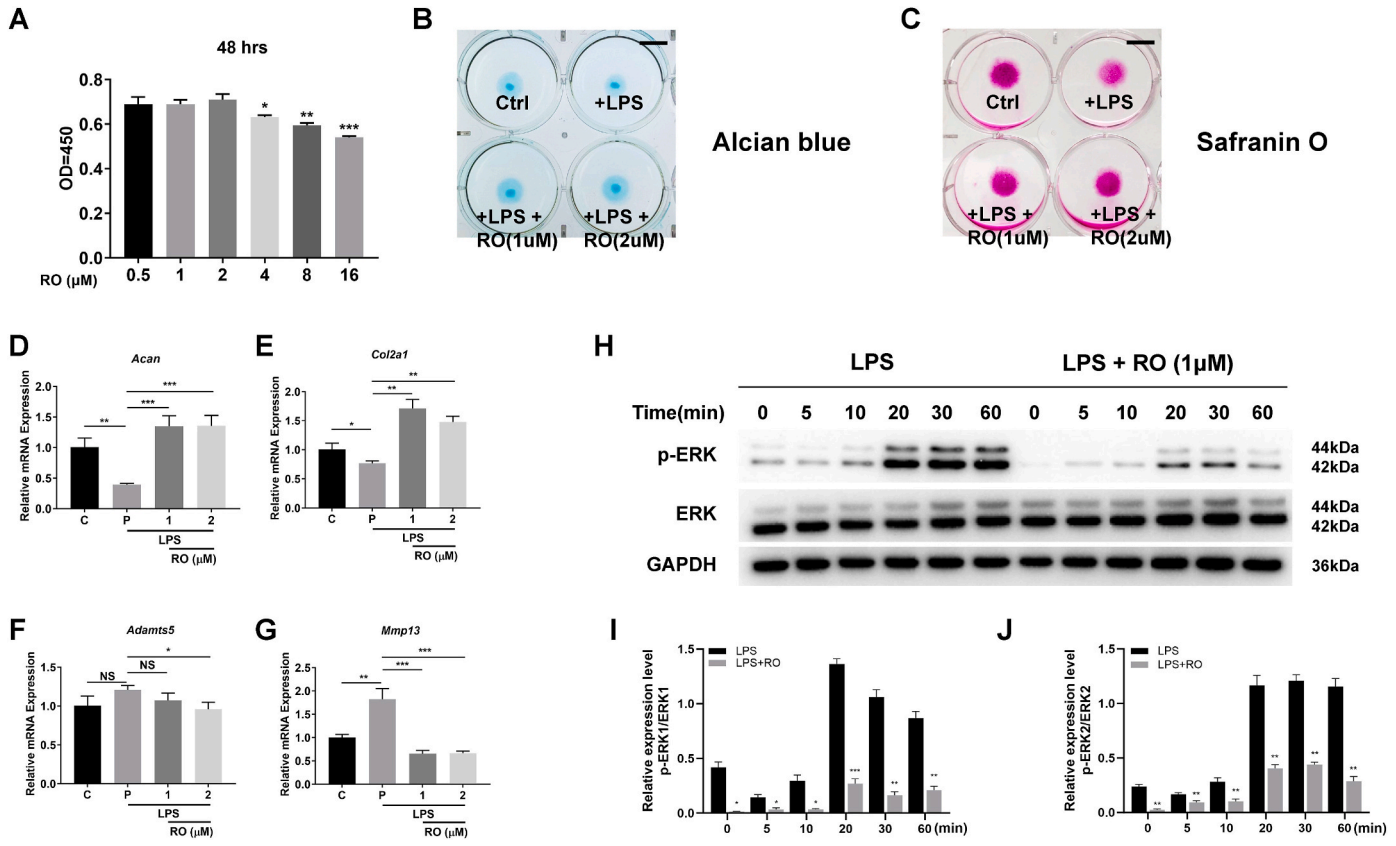

Fig. 5. RO inhibited inflammation of chondrocytes by inhibiting LPS-induced activation of the ERK pathway. (**A**) Toxicity detection of RO for chondrocytes at 48h. (**B-C**) Examine the effect of RO(1 μM,2 μM) on LPS-induced chondrocyte degeneration with Alcian Blue (**B**), and Safranin O staining (**C**). Scale bar = 1 mm. (**D-G**) Quantification of *Acan* (**D**), *Col2a1* (**E**), *Adamts5* (**F**) and *Mmp13* (**G**) with β-actin used as a control, in chondrocytes incubated with RO and LPS. (**H-J**) ATDC5s were pretreated with or without RO (20 nM) for 3h and then stimulated with LPS (2 μg/mL) for indicated time period (0, 5, 10, 20, 30, 60 min), and the cell lysates were quantitatively analyzed using western blot for ERK signaling pathways. Data represent mean ± SD. N = 3 per group; *p < 0.05, **p < 0.01, ***p < 0.001.

3.4. RO inhibits RANKL-induced activation of ERK/c-fos/NFATc1 pathway

The two important transcription factors, NFATc1 and c-fos, and the protein kinases associated with the MAPK signaling pathway (such as ERK, JNK and p38) fulfilled important roles in osteoclast formation [37,38]. Previous studies have shown that ERK, JNK, and other pathways exhibit distinct activation peaks within the first hour of RANKL treatment [39,40]. Therefore, we selected 0, 5, 10, 20, 30, and 60 min as time points to capture the signaling pathway's dynamic activation. As demonstrated by western blotting, pretreatment with 20 nM RO significantly inhibited the expression of p-ERK1/2 after RANKL stimulation, but had no influence on p-JNK or p-p38 expression (Fig. 4A–D). NFATc1 and c-fos are regulated by the ERK signaling pathway and are required for osteoclast fusion [15,41]. After using 20 nM RO, the expression of NFATc1 and c-fos was significantly reduced (Fig. 4E and F). Taken together, these findings demonstrate that RO impedes osteoclast fusion by suppressing RANKL-mediated activation of the ERK/c-fos/NFATc1 axis.

3.5. RO blocks inflammation of chondrocytes and enhances chondrocyte autophagy by inhibiting LPS-induced activation of the ERK pathway

To analyze the effect of RO on OA degeneration in LPS-treated chondrocytes, we determined RO cytotoxicty using CCK-8 assay, and found that concentrations ≤ 2 μM was non-toxic to chondrocytes (Fig. 5A). Then, we examined the effect of RO by staining with alcian blue, and safranin O. It showed that RO restrained the inflammatory degeneration of chondrocytes effectively (Fig. 5B and C). Additionally, genes associated with inflammatory degeneration were detected [42]. Assessment of anabolism marker (*Acan and Col2a1*), and catabolism markers (*Adamts5 and Mmp13*) with qPCR showed higher levels of *Acan* and *Col2a1* and significantly decreased in *Mmp13* mRNA in LPS-treated chondrocytes incubated with RO, with similar decrease observed in *Adamts5* (Fig. 5D–G). Then, pretreatment with 2 μM RO significantly inhibited the expression of p-ERK1/2 LPS stimulation (Fig. 5H–J). Additionally, qPCR results revealed that IL-1β, IL-6, and TNF-α expression levels in chondrocytes treated with RO were significantly reduced compared to the LPS group (Supplementary Figure 1). These results demonstrate that RO suppressed LPS-induced inflammation of chondrocytes via the ERK signaling pathway.

To investigate how RO regulates ERK signaling in OA, we performed Western blot analysis of autophagy-related proteins in chondrocytes treated with LPS and subsequently with RO. Chondrocytes treated with LPS alone showed significantly higher P62 protein expression (Fig. 6E,F) and a lower LC3-II/LC3-I ratio compared to other groups (Fig. 6E,G). RO treatment reduced P62 protein expression and significantly increased the LC3-II/LC3-I ratio in chondrocytes. These findings suggest that RO promotes chondrocyte autophagy by inhibiting the ERK signaling pathway, which may slow arthritis progression. To confirm the mechanism at the histological level, we performed IHC staining on joint sections from ACLT mouse models. IHC results showed that ACLT-induced arthritis led to a significant decrease in COL2A1 and LC3B expression, along with increased p-ERK levels. RO treatment effectively inhibited p-ERK in both low-dose and high-dose groups, while significantly increasing COL2A1 and LC3B expression (Fig. 6A–D). These findings confirm that RO enhances chondrocyte autophagy by inhibiting the ERK signaling pathway, which helps mitigate OA progression.

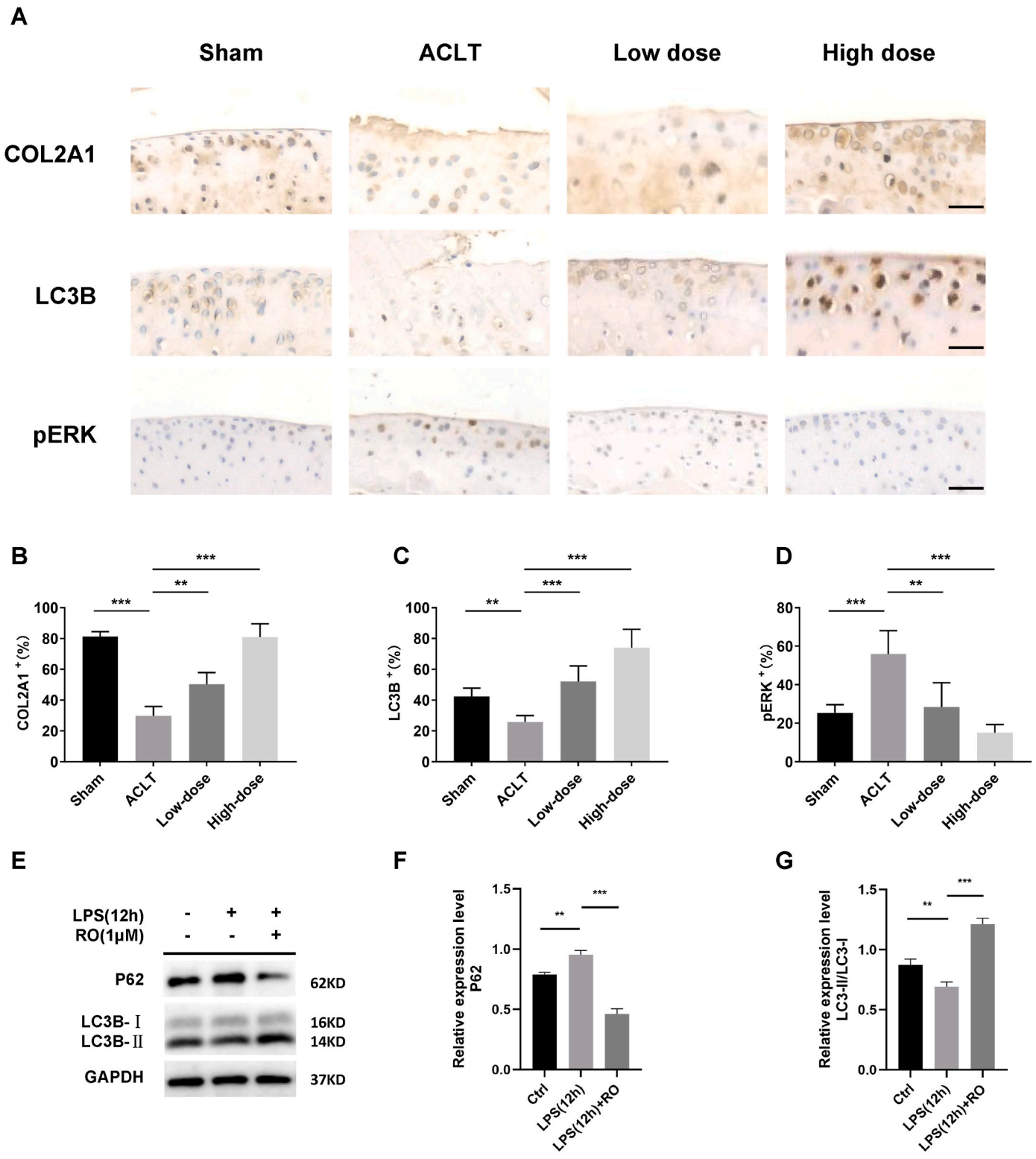

Fig. 6. RO enhanced chondrocyte autophagy and mitigates cartilage degeneration in ACLT mice. (**A**) IHC staining of COL2A1, LC3B and pERK in the knee cartilage of mice at 6 weeks after ACLT surgery. Scale bar = 50 μm; (**B-D**) Quantitative analysis for IHC staining; (**E-G**) ATDC5s were pretreated with or without RO (20 nM) for 3h and then stimulated with LPS (2 μg/mL) for 12h, and the cell lysates were quantitatively analyzed using western blot for P62 and LC3B signaling pathways. Data represent mean ± SD. N = 3 per group; $p < 0.05$, **$p < 0.01$, ***$p < 0.001$. High-dose: 5 mg/kg, and Low-dose: 1 mg/kg.

3.6. The ERK signaling pathway is significantly upregulated in human OA

To investigate the signaling pathways in human OA, we analyzed published single-cell data from articular cartilage tissues, comprising 3 normal samples and 16 OA samples. Following quality filtering of the raw data, we identified 133,337 high-quality cells (Fig. 7A). Utilizing the Harmony R package for integration, we clustered the cells into 4 distinct populations (Fig. 7A and B): articular chondrocytes (ArtiChon, marker genes: *ACAN*, *COL2A1*, *SOX9*, *PRG4*), osteoblasts (OsteoB, marker genes: *BGLAP*, *RUNX2*, *ALPL*), endothelial cells (Endo, marker

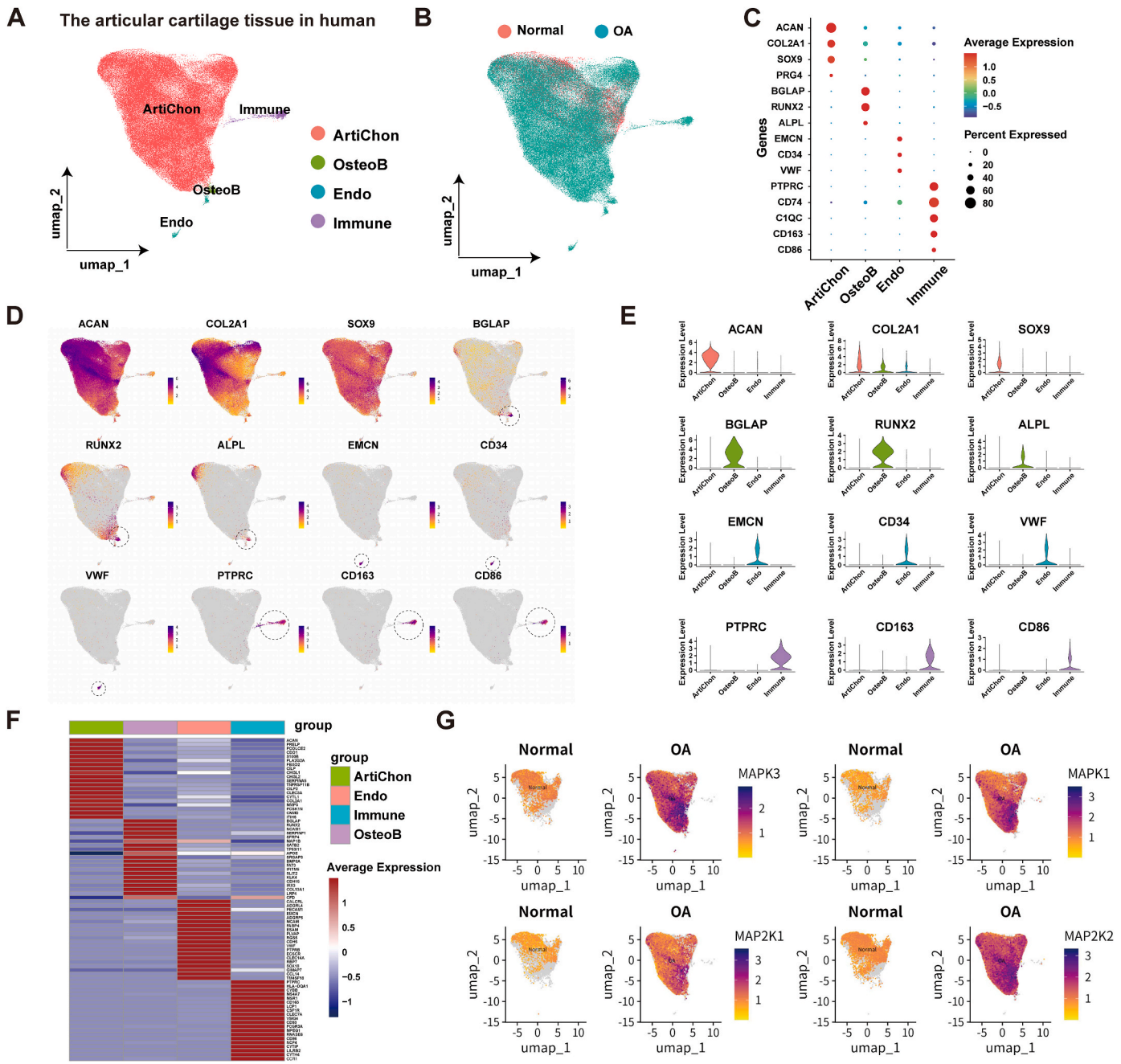

Fig. 7. scRNA-seq analysis reveals significant upregulation of ERK1/2 in human OA. (**A**) UMAP plot of single-cell data from human articular cartilage tissue, showing four distinct cell clusters: ArtiChon (articular chondrocytes, red), OsteoB (osteoblasts, green), Endo (endothelial cells, cyan), and Immune (immune cells, purple). (**B**) UMAP plot of integrated data using harmony, including samples from 3 healthy individuals and 16 arthritis patients. (**C-E**) Dotsplot, FeaturePlot, and violinplot shows marker genes for each cluster. (**F**) A heatmap displaying the top 20 significantly different genes in each group, with red indicating high average expression and blue representing low average expression. (**G**) UMAP plots comparing the expression of ERK and MEK pathway genes (*MAPK3* [ERK1], *MAPK1* [ERK2], *MAP2K1* [MEK1], *MAP2K2* [MEK2]), showing significantly higher expression in OA patients.

genes: *EMCN*, *CD34*, *VWF*), and immune cells (Immune, marker genes: *PTPRC*, *CD74*, *C1QC*, *CD163*, *CD86*). We employed dotsPlot, featurePlot, and violinPlot to qualitatively and quantitatively display marker gene expression and distribution (Fig. 7C–E). Heatmaps of the top 20 differentially expressed genes (DEGs) in each group highlighted key roles of specific genes. Articular chondrocytes exhibited elevated expression of *ACAN*, *COL2A1*, *CILP*, *CHI3L1*, and *PCOLCE2*, indicative of active cartilage matrix formation and maintenance. Endothelial cells showed high levels of *PECAM1*, *VWF*, *SOX18*, *ESAM*, and *MCAM*, underscoring their roles in cell interactions, blood coagulation, and angiogenesis. Osteoblasts were characterized by *RUNX2*, *BGLAP*, *SATB2*, *SFRP4*, and *BMP8A*, essential for bone formation and metabolism. Immune cells displayed hightened expression of *CD86*, *PTPRC*, *CD163*, *CSF1R*, and *HLA-DQA1*, suggesting active involvement in immune responses (Fig. 7F). Notably, OA samples demonstrated increased expression of *MAPK3* (ERK1), *MAPK1* (ERK2), *MAP2K1* (MEK1), and *MAP2K2* (MEK2), indicating upregulation of the ERK and MEK pathways (Fig. 6G). Analysis of the top 100 DEGs between OA and normal samples revealed significant enrichment of ERK-related signaling pathways, including Signaling to ERKs, ERK/MAPK targets, MAP2K and MAPK activation, MAPK family signaling cascades, and Prolonged ERK activation events (Fig. 8A). Furthermore, GSEA demonstrated significant

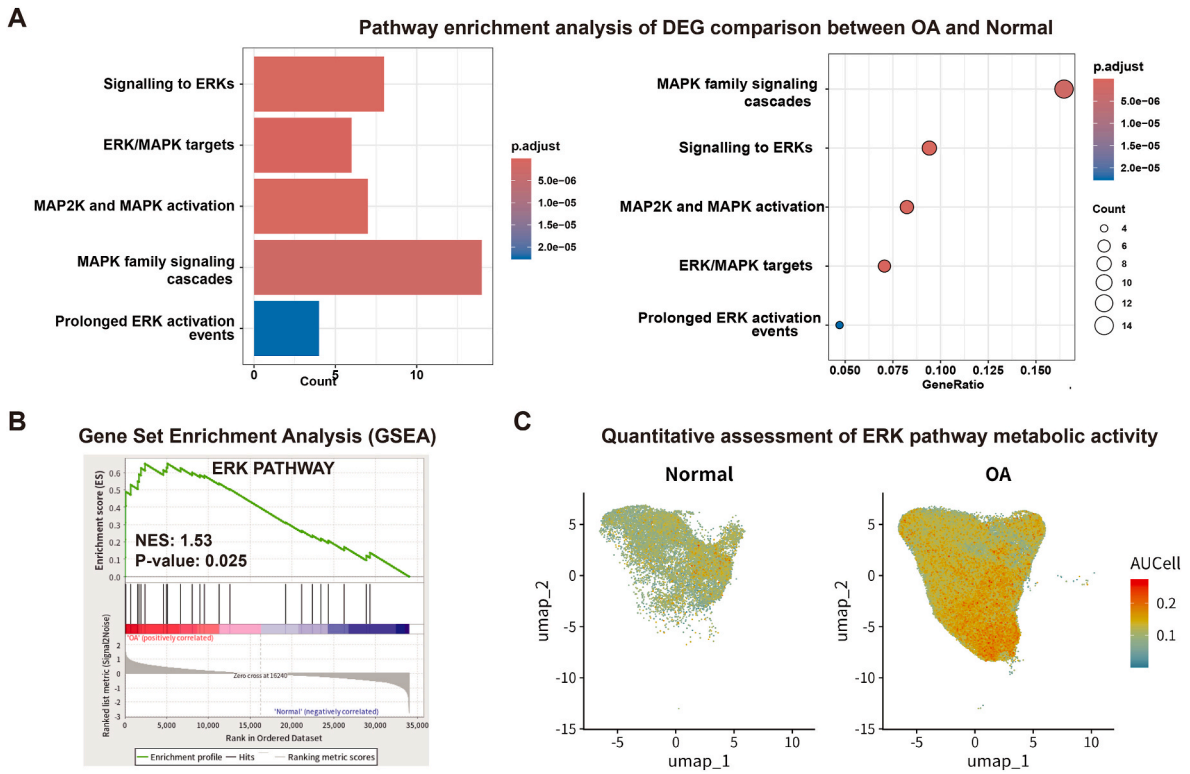

Fig. 8. ERK pathway enrichment in OA vs. normal tissues. (**A**) Dot plots depict the relative expression levels, and bar plots illustrate the statistical significance of enrichment. (**B**) GSEA analysis indicates that the ERK pathway is highly enriched in arthritis samples. (**C**) Quantitative assessment of ERK pathway metabolic activity using scMetabolism shows significantly higher AUCell scores in OA patients compared to healthy individuals.

enrichment of the ERK pathway in OA (P-value: 0.025, NES: 1.53) (Fig. 8B). Quantitative assessment of ERK pathway metabolic activity using the scMetabolism R package revealed significantly higher AUCell scores in arthritis patients compared to healthy individuals (Fig. 8C). In particular, we focused on the clusters of macrophages (marker genes: C1QA, CD86, CD163) and osteoclasts (marker genes: CTSK, ACP5, TNFRSF11A). GO enrichment analysis revealed a significant upregulation of ERK-related pathways in macrophages. GSVA analysis of GO terms and pathways also showed upregulation of the ERK pathway in both macrophages and osteoclasts (Supplementary Figure 3). In conclusion, the ERK/MAPK signaling pathway likely plays a critical role in OA pathogenesis by promoting abnormal proliferation, differentiation, inflammatory responses, and extracellular matrix degradation in chondrocytes.

4. Discussion

OA is hard to cure due to our lack of comprehensive understanding of the pathogenesis of OA [43,44]. Currently, clinical use of OA drugs can only relieve the symptoms of OA, but do not delay the progression of the disease. Multiple studies have shown that RO is able to inhibit RAF and MEK at the same time, which subsequently inhibit ERK pathway [18, 45]. Based on these findings, we hypothesized that RO may play an important role in OA treatment.

OA is a disease that affects all joints. Articular cartilage and subchondral bone are jointly involved in the occurrence and development of OA by constituting a structural and functional unit [8,14]. In the early stage of OA, overactivation of osteoclasts leads to erosion and remodeling of subchondral bone, which leads to degeneration of cartilage in late stage of OA [13,46]. In the present study, we established an OA model using the ACLT method [47]. Micro-CT scanning showed the damage and erosion of subchondral bone after ACLT, which was consistent with an increase in the number of osteoclasts stained by TRAP in subchondral bone. At the same time, the degeneration of cartilage was confirmed by HE staining and Safranin O-Fast Green staining. However, the application of RO inhibits bone loss in subchondral bone and mitigated the degeneration of articular cartilage, thus suppressing OA progression and attenuating OA development.

For molecular mechanism, first of all, we found that RO hindered the fusion of osteoclasts. During osteoclastogenesis, mononucleated preosteoclasts derived from the monocyte/macrophage lineage fuse into multinucleated osteoclasts [48,49]. RANKL initiates the activation of extracellular signal-regulated kinase (ERK) and subsequently induces, in turn, two important transcription factors for osteoclast fusion: c-fos and NFATc1 [37,38,50]. RO effectively eliminated the overactivation of osteoclasts in subchondral bone by inhibiting the ERK/c-fos/NFATc1 pathway. At the same time, ERK is also associated with cartilage calcification and osteophyte formation [19,51]. We demonstrated that RO effectively inhibits LPS-induced inflammatory degeneration of chondrocytes and promotes chondrocyte autophagy by blocking the ERK pathway in osteoarthritis treatment.

The study also has some limitations. First, all mice used in this experiment were young and male. In order to further study the protective effects of RO on articular cartilage subchondral bone and articular cartilage, it is necessary to evaluate its effects on female, obese, and age-related OA mouse models [52]. Second, the evaluation of OA and its associated mechanisms was undertaken using ACLT model, which does not adequately cover all aspects of OA. To verify the therapeutic effect of RO in OA, long-term studies involving *in vivo* and *in vitro* experiments in other models are required. Third, while this study demonstrated the potential of RO in treating OA by inhibiting the ERK pathway, its extensive signaling role limits the ability to specifically target OA. In future OA treatments, RO could be specifically delivered to pathological tissues using antibody-drug conjugates or nanoparticle-mediated targeting. This approach could enhance the specificity and effectiveness of OA treatment. This study is mainly focused on osteoclastogenesis was

mainly studied, and the mechanism of RO in osteoclast precursor migration needs to be further explored.

In conclusion, we revealed the role of RO in OA treatment for the first time, demonstrated *in vivo* that RO can inhibit OA progression through mouse ACLT model, and demonstrated that RO can delay OA degeneration *in vitro* through BMMs and ATDC5. In addition, we found that RO may inhibit osteoclast differentiation and bone absorption function by inhibiting the ERK/c-fos/NFATc1 pathway, and significantly block the inflammatory degeneration of chondrocytes and promotes chondrocyte autophagy by inhibiting the ERK pathway. Furthermore, we analyzed the published single-cell data from humans and confirmed the significant upregulation of the ERK signaling pathway in human OA. All these evidences suggest that RO is a potential new OA treatment drug and has important guiding significance for the development of new drugs for OA.

Ethics statement

The animal study was reviewed and approved by Ethics Committee of the Xiamen University.

CRediT authorship contribution statement

Han Wang: Conceptualization, Supervision, Data curation. **Xiwen Yuan:** Investigation, Data curation, Writing – original draft. **Jie Han:** Software, Writing – original draft. **Zuoxing Wu:** Data curation, Writing – review & editing. **Zheru Ma:** Data curation, Writing – review & editing. **Fan Shi:** Data curation. **Zhengqiong Luo:** Data curation. **Zihan Chen:** Data curation. **Chenyang Guo:** Writing – review & editing. **Guixin Yuan:** Writing – review & editing. **Xuemei He:** Data curation. **Zemin Ling:** Supervision, Writing – review & editing. **Lin Meng:** Conceptualization, Formal analysis. **Rong Shen:** Investigation, Writing – review & editing. **Jianming Huang:** Investigation, Writing – review & editing. **Ren Xu:** Conceptualization, Writing – review & editing.

Conflict of interest

The authors declare that they have no competing interests.

Acknowledgements

This work was supported by National Natural Science Foundation of China (92468203, 82372362, 81972034, 92068104 to RX, and 82102520 to ZML), Natural Science Foundation of Fujian Province (2022J06003 to RX) and Project of Xiamen Cell Therapy Research (Grant No. 3502Z20214001). The graphical abstract was created with BioRender.com.

Appendix A. Supplementary data

Supplementary data to this article can be found online at https://doi.org/10.1016/j.jot.2025.03.002.

References

[1] Tong L, Yu H, Huang X, Shen J, Xiao G, Chen L, et al. Current understanding of osteoarthritis pathogenesis and relevant new approaches. Bone Res 2022;10(1):60.
[2] Chen D. Osteoarthritis: a complicated joint disease requiring extensive studies with multiple approaches. J Orthop Translat 2022;32:130.
[3] Katz JN, Arant KR, Loeser RF. Diagnosis and treatment of hip and knee osteoarthritis: a review. JAMA 2021;325(6):568–78.
[4] Diseases GBD, Injuries C. Global burden of 369 diseases and injuries in 204 countries and territories, 1990-2019: a systematic analysis for the Global Burden of Disease Study 2019. Lancet 2020;396(10258):1204–22.
[5] Long H, Liu Q, Yin H, Wang K, Diao N, Zhang Y, et al. Prevalence trends of site-specific osteoarthritis from 1990 to 2019: findings from the global burden of disease study 2019. Arthritis Rheumatol 2022;74(7):1172–83.
[6] Bruyere O, Cooper C, Arden N, Branco J, Brandi ML, Herrero-Beaumont G, et al. Can we identify patients with high risk of osteoarthritis progression who will respond to treatment? A focus on epidemiology and phenotype of osteoarthritis. Drugs Aging 2015;32(3):179–87.
[7] Zhang Z, Huang C, Jiang Q, Zheng Y, Liu Y, Liu S, et al. Guidelines for the diagnosis and treatment of osteoarthritis in China (2019 edition). Ann Transl Med 2020;8(19):1213.
[8] Goldring SR, Goldring MB. Changes in the osteochondral unit during osteoarthritis: structure, function and cartilage-bone crosstalk. Nat Rev Rheumatol 2016;12(11):632–44.
[9] Kim BJ, Koh JM. Coupling factors involved in preserving bone balance. Cell Mol Life Sci 2019;76(7):1243–53.
[10] Sims NA, Martin TJ. Osteoclasts provide coupling signals to osteoblast lineage cells through multiple mechanisms. Annu Rev Physiol 2020;82:507–29.
[11] Li G, Ma Y, Cheng TS, Landao-Bassonga E, Qin A, Pavlos NJ, et al. Identical subchondral bone microarchitecture pattern with increased bone resorption in rheumatoid arthritis as compared to osteoarthritis. Osteoarthr Cartil 2014;22(12):2083–92.
[12] Lin C, Liu L, Zeng C, Cui ZK, Chen Y, Lai P, et al. Activation of mTORC1 in subchondral bone preosteoblasts promotes osteoarthritis by stimulating bone sclerosis and secretion of CXCL12. Bone Res 2019;7:5.
[13] Ma L, Zhao X, Liu Y, Wu J, Yang X, Jin Q. Dihydroartemisinin attenuates osteoarthritis by inhibiting abnormal bone remodeling and angiogenesis in subchondral bone. Int J Mol Med 2021;47(3).
[14] Guo H, Ding D, Wang L, Yan J, Ma L, Jin Q. Metformin attenuates osteoclast-mediated abnormal subchondral bone remodeling and alleviates osteoarthritis via AMPK/NF-kappaB/ERK signaling pathway. PLoS One 2021;16(12):e0261127.
[15] Fang C, Guo JW, Wang YJ, Li XQ, Zhang H, Cui J, et al. Diterbutyl phthalate attenuates osteoarthritis in ACLT mice via suppressing ERK/c-fos/NFATc1 pathway, and subsequently inhibiting subchondral osteoclast fusion. Acta Pharmacol Sin 2022;43(5):1299–310.
[16] Wang Z, Zhang Z, Zhao J, Yong C, Mao Y. Polysaccharides from enteromorpha prolifera ameliorate acute myocardial infarction in vitro and in vivo via up-regulating HIF-1alpha. Int Heart J 2019;60(4):964–73.
[17] White SM, Avantaggiati ML, Nemazanyy I, Di Poto C, Yang Y, Pende M, et al. YAP/TAZ inhibition induces metabolic and signaling rewiring resulting in targetable vulnerabilities in NF2-deficient tumor cells. Dev Cell 2019;49(3):425–443 e9.
[18] Martinez-Garcia M, Banerji U, Albanell J, Bahleda R, Dolly S, Kraeber-Bodere F, et al. First-in-human, phase I dose-escalation study of the safety, pharmacokinetics, and pharmacodynamics of RO5126766, a first-in-class dual MEK/RAF inhibitor in patients with solid tumors. Clin Cancer Res 2012;18(17):4806–19.
[19] Lin Z, Miao J, Zhang T, He M, Wang Z, Feng X, et al. JUNB-FBXO21-ERK axis promotes cartilage degeneration in osteoarthritis by inhibiting autophagy. Aging Cell 2021;20(2):e13306.
[20] Chen G, Zhao H, Ma S, Chen L, Wu G, Zhu Y, et al. Circadian rhythm protein Bmal1 modulates cartilage gene expression in temporomandibular joint osteoarthritis via the MAPK/ERK pathway. Front Pharmacol 2020;11:527744.
[21] Li M, Xiao YB, Wang XT, Zhuang JP, Zhou CL. Proline-serine-threonine phosphatase-interacting protein 2 alleviates diabetes mellitus-osteoarthritis in rats through attenuating synovial inflammation and cartilage injury. Orthop Surg 2021;13(4):1398–407.
[22] Nakamura I, Takahashi N, Jimi E, Udagawa N, Suda T. Regulation of osteoclast function. Mod Rheumatol 2012;22(2):167–77.
[23] Vina ER, Kwoh CK. Epidemiology of osteoarthritis: literature update. Curr Opin Rheumatol 2018;30(2):160–7.
[24] Tschon M, Contartese D, Pagani S, Borsari V, Fini M. Gender and sex are key determinants in osteoarthritis not only confounding variables. A systematic review of clinical data. J Clin Med 2021;10(14).
[25] Yan YS, Qu Z, Yu DQ, Wang W, Yan S, Huang HF. Sex steroids and osteoarthritis: a mendelian randomization study. Front Endocrinol 2021;12:683226.
[26] Cui Z, Crane J, Xie H, Jin X, Zhen G, Li C, et al. Halofuginone attenuates osteoarthritis by inhibition of TGF-beta activity and H-type vessel formation in subchondral bone. Ann Rheum Dis 2016;75(9):1714–21.
[27] Xu R, Zhang C, Shin DY, Kim JM, Lalani S, Li N, et al. c-Jun N-terminal kinases (JNKs) are critical mediators of osteoblast activity in vivo. J Bone Miner Res 2017;32(9):1811–5.
[28] Greenblatt MB, Park KH, Oh H, Kim JM, Shin DY, Lee JM, et al. CHMP5 controls bone turnover rates by dampening NF-kappaB activity in osteoclasts. J Exp Med 2015;212(8):1283–301.
[29] Kusumbe AP, Ramasamy SK, Starsichova A, Adams RH. Sample preparation for high-resolution 3D confocal imaging of mouse skeletal tissue. Nat Protoc 2015;10(12):1904–14.
[30] Livak KJ, Schmittgen TD. Analysis of relative gene expression data using real-time quantitative PCR and the 2(-Delta Delta C(T)) Method. Methods 2001;25(4):402–8.
[31] Kong YY, Yoshida H, Sarosi I, Tan HL, Timms E, Capparelli C, et al. OPGL is a key regulator of osteoclastogenesis, lymphocyte development and lymph-node organogenesis. Nature 1999;397(6717):315–23.
[32] Yeon JT, Kim KJ, Choi SW, Moon SH, Park YS, Ryu BJ, et al. Anti-osteoclastogenic activity of praeruptorin A via inhibition of p38/Akt-c-Fos-NFATc1 signaling and PLCgamma-independent Ca2+ oscillation. PLoS One 2014;9(2):e88974.
[33] Fan Y, Bian X, Meng X, Li L, Fu L, Zhang Y, et al. Unveiling inflammatory and prehypertrophic cell populations as key contributors to knee cartilage degeneration in osteoarthritis using multi-omics data integration. Ann Rheum Dis 2024;83(7):926–44.
[34] Zhang X, Wang C, Zhao J, Xu J, Geng Y, Dai L, et al. miR-146a facilitates osteoarthritis by regulating cartilage homeostasis via targeting Camk2d and Ppp3r2. Cell Death Dis 2017;8(4):e2734.

[35] Veis DJ, O'Brien CA. Osteoclasts, master sculptors of bone. Annu Rev Pathol 2023; 18:257–81.
[36] Yang C, Tao H, Zhang H, Xia Y, Bai J, Ge G, et al. TET2 regulates osteoclastogenesis by modulating autophagy in OVX-induced bone loss. Autophagy 2022;18(12): 2817–29.
[37] Grigoriadis AE, Wang ZQ, Cecchini MG, Hofstetter W, Felix R, Fleisch HA, et al. c-Fos: a key regulator of osteoclast-macrophage lineage determination and bone remodeling. Science 1994;266(5184):443–8.
[38] Takayanagi H. The role of NFAT in osteoclast formation. Ann N Y Acad Sci 2007; 1116:227–37.
[39] Zhou S, Li J, Ying T, Wang Y, Wang Q, Li X, et al. StemRegenin 1 attenuates the RANKL-induced osteoclastogenesis via inhibiting AhR-c-src-NF-kappaB/p-ERK MAPK-NFATc1 signaling pathway. iScience 2024;27(5):109682.
[40] Li L, Yang M, Shrestha SK, Kim H, Gerwick WH, Soh Y. Kalkitoxin reduces osteoclast formation and resorption and protects against inflammatory bone loss. Int J Mol Sci 2021;22(5).
[41] Chen K, Qiu P, Yuan Y, Zheng L, He J, Wang C, et al. Pseurotin A inhibits osteoclastogenesis and prevents ovariectomized-induced bone loss by suppressing reactive oxygen species. Theranostics 2019;9(6):1634–50.
[42] Chen YH, Zhang X, Chou CH, Hsueh MF, Attarian D, Li YJ, et al. Association of dipeptidylpeptidase 4 (CD26) with chondrocyte senescence and radiographic progression in knee osteoarthritis. Arthritis Rheumatol 2023;75(7):1120–31.
[43] Wu H, Xu T, Chen Z, Wang Y, Li K, Chen PS, et al. Specific inhibition of FAK signaling attenuates subchondral bone deterioration and articular cartilage degeneration during osteoarthritis pathogenesis. J Cell Physiol 2020;235(11): 8653–66.
[44] Ji ML, Jiang H, Li Z, Geng R, Hu JZ, Lin YC, et al. Sirt6 attenuates chondrocyte senescence and osteoarthritis progression. Nat Commun 2022;13(1):7658.
[45] Akinleye A, Furqan M, Mukhi N, Ravella P, Liu D. MEK and the inhibitors: from bench to bedside. J Hematol Oncol 2013;6:27.
[46] Ziemian SN, Witkowski AM, Wright TM, Otero M, van der Meulen MCH. Early inhibition of subchondral bone remodeling slows load-induced posttraumatic osteoarthritis development in mice. J Bone Miner Res 2021;36(10):2027–38.
[47] Wang G, Chen S, Xie Z, Shen S, Xu W, Chen W, et al. TGFbeta attenuates cartilage extracellular matrix degradation via enhancing FBXO6-mediated MMP14 ubiquitination. Ann Rheum Dis 2020;79(8):1111–20.
[48] Kodama J, Kaito T. Osteoclast multinucleation: review of current literature. Int J Mol Sci 2020;21(16).
[49] Pereira M, Petretto E, Gordon S, Bassett JHD, Williams GR, Behmoaras J. Common signalling pathways in macrophage and osteoclast multinucleation. J Cell Sci 2018; 131(11).
[50] Boyle WJ, Simonet WS, Lacey DL. Osteoclast differentiation and activation. Nature 2003;423(6937):337–42.
[51] Prasadam I, Mao X, Shi W, Crawford R, Xiao Y. Combination of MEK-ERK inhibitor and hyaluronic acid has a synergistic effect on anti-hypertrophic and pro-chondrogenic activities in osteoarthritis treatment. J Mol Med (Berl) 2013;91(3): 369–80.
[52] Lin Z, Miao J, Zhang T, He M, Zhou X, Zhang H, et al. d-Mannose suppresses osteoarthritis development in vivo and delays IL-1beta-induced degeneration in vitro by enhancing autophagy activated via the AMPK pathway. Biomed Pharmacother 2021;135:111199.